Research Square

Preprints are preliminary reports that have not undergone peer review.
They should not be considered conclusive, used to inform clinical practice,
or referenced by the media as validated information.

Experimental and theoretical study of Mg doped SnO nanoparticles used for the efficient photocatalytic degradation of Methyl violet dye under UV assisted light

Nisar Khan
Bacha Khan University
Tamanna Gul
Bacha Khan University Charsadda
Falak Naz
Bacha Khan University Charsadda
Wilayat Khan
Bacha Khan University Charsadda
Sikander Azam
Ripha International University Islamabad
Khalid Saeed
khalidkhalil2002@yahoo.com

Bacha Khan University Charsadda

Research Article

Keywords: Mg doped SnO NPs, Methyl violet dye, Photodegradation, DFT

Posted Date: June 3rd, 2026

DOI: https://doi.org/10.21203/rs.3.rs-9897122/v1

License: This work is licensed under a Creative Commons Attribution 4.0 International License.
Read Full License

Additional Declarations: The authors declare no competing interests.

Experimental and theoretical study of Mg doped SnO nanoparticles used for the efficient photocatalytic degradation of Methyl violet dye under UV assisted light

[1]Nisar Khan, [1]Tamanna Gul, [1]Falak Naz, [2] Wilayat Khan, [3]Sikander Azam, [1]Khalid Saeed*

[1]Department of Chemistry, Bacha Khan University Charsadda, Charsadda, Khyber Pakhtunkhwa, Pakistan

[2]Department of Physics, Bacha Khan University Charsadda, Charsadda, Khyber Pakhtunkhwa Pakistan

[3]Department of Physics, Riphah International University Islamabad, Islamabad, Pakistan

*Corresponding author:

Email: khalidkhalil2002@yahoo.com; khalidsaeed@bkuc.edu.pk

Abstract

The treatment of wastewater with organic dyes is a crucial issue to reduce water pollution. This study modeled Mg-doped SnO nanoparticles using density functional theory (DFT) and analyzed them using the full-potential linearized augmented plane wave (FP-LAPW) employed in the WIEN2k simulation programming code. Further, the theoretically modeled nanoparticles (NPs) were synthesized via the co-precipitation method, which is an efficient photocatalyst for the photodegradation of methyl violet (MV) dye. The morphological study showed that the shape of NPs are cubic and round while the average size of agglomerated NPs is below 440 nm. Density functional calculations were also performed to investigate the role of Mg in the band gap engineering of SnO. The calculated optical band gap from UV-vis spectroscopy and DFT calculations is 3.0 eV and 2.94 eV, respectively. The calculated band structure of pristine SnO reveals the fundamental band gap value of 1.129 eV, whereas the Mg atom contributes a localized band exposed in the doped SnO. The photodegradation study illustrated that Mg-doped SnO NPs degraded 99.3% of MV dye within 25 min under UV irradiation. It was also found that the recovered and re-recovered NPs were also significantly degraded the MV dye. The recovered and re-recovered Mg doped SnO NPs photodegraded about 52 and 73% MV within 25 min. The impact of other of parameters like NPs dosage, pH of medium and initial dye concentration on the photodegradation of dye was also examined. Moreover, Kinetic analysis shows that the photodegradation of MV dye follows pseudo first order reaction.

Key words: Mg doped SnO NPs, Methyl violet dye, Photodegradation, DFT

1. Introduction

Organic pollutants are chemically stable compounds that are commonly ffound in the aquatic environment (Du et al. 2022). Different industries released effluents, which mainly contain organic dye (Cheng et al. 2022). Dyes are synthetic and natural colored compounds, when it is applied to a substrate form chemical bond with it (Bai et al. 2021). Dyes are accessible mainly in non-ionic, anionic and cationic form. Anionic dyes include acid, direct and reactive dye, while dispersive and basic dyes are referred to non ionic and cationic dyes, respectively (Kadhom 2020). Based on functional groups, dyes may also be classified into sulfur, azo, anthraquinone and indigo dye etc. (Benkhayaa et al. 2020). Dyes are extensively used in coating, rubber, food, painting, automotive, drugs, textiles, pulp, cosmetics, sugar etc. industries (Gul et al. 2023; Pirzada et al. 2021). Majority of them (organic dyes) are teratogenic, carcinogenic, toxic, non-biodegradable and xenobiotic due to their intricate chemical structure and bulky size, which provide risk to aquatic and human life (Aljuaid et al. 2023). Human liver, eyes, chromosome, skin, kidney, enzymatic, central nerve system and reproductive system are greatly influenced through dye (Haleem et al. 2023). According to the latest reports; approximately 175,000 tons of dye is randomly discharge into world's water supplies per year (Kumari et al. 2023). In cotton industries, the reactive dye concentration is reported as 60 mg L^{-1} (Yaseen et al. 2019). Among dyes, MV is a toxic and type of cationic dye. MV dye has dark blue color in water and show high stability against oxidizing agent, aerobic assault and photolysis through sunlight. MV dye is used in printing, rubber, textile and leather industries. In chemical and biological labs, MV dye are frequently utilized as pH indicator, bactericidal and antiallergenic agent. MV dye is common irritant that can harm the respiratory system, skin, eyes, liver and gastrointestinal tract of human [Afzal et al. 2023;, Hamza et al. 2009). Furthermore, in the aquatic environment, MV dye inhibit the growth of microbes,

plants and has detrimental effect on photosynthetic processes (Al-Tohamy et al.2022). MV dye can be removed from the industrials effluents by using variety of techniques like biodegradation (Leilakouhi et al. 2023), coagulation (Moradkhanloo et al. 2023), flocculation (Quintero et al. 2024), ultrafiltration (Oyarce et al. 2021), reverse osmosis (Saini et al. 2023), ion exchange (Abdallah and Alprol 2024), nano filtration (Elfiky et al. 2024), electro coagulation (. Negash et al 2023) and advanced oxidation (Ledakowicz and Pa´zdzi 2021). These classical approaches/methods are challenging to manage, non-destructive, expansive and only result in the transfer of pollutant material into sludge and the creation of new kind of pollution that requires additional treatment (Khan et al. 2024). Currently, advanced oxidation processes receiving great attention due to their easy operation, moderate reaction condition and cost effectiveness (Wang et al. 2022). Photocatalytic degradation an effective technique for the treatment of waste water, where semiconductor metals oxides NPs are use as photocatalyst, which present considerable activity for the breakdown of non-degradable dyes (Karthik et al. 2022). Photocatalytic degradation is superior as compared to other conventional techniques due to the complete mineralization of pollutants, economical, ease of uses, and the potential to perform the processes at normal temperature and pressure (Sabouri et al. 2023; Saeed et al. 2023). This technique requires, the light sources, oxygen, and semiconductor NPs (Mecha et al. 2020). During photodegradation process, different photocatalysts like Mn, Mg doped ZrO_2 (Vignesh et al. 2021), Cu doped ZnO (Rezeki and Zainul 2024), Ni doped SnO (Kaur et al. 2024), Fe doped CdO (Mandal et al. 2021), $KCoPO_4$ (Bagtache et al. 2022), $HOVO_4$-CuO nanocomposite (Khorasanizadehet al. 2022), $FePO_4$ (Benomara et al. 2021) and Fe_3O_4 MNPs (Keyhanian et al. 2016) etc. were employed.

In the current study, Mg-doped SnO NPs were prepared via the co-precipitation method, along with density functional simulation was used to indicate the importance of Mg on the electronic and

optical properties. The Mg doped SnO NPs were characterized by FT-IR, SEM, EDX and XRD. These prepared Mg doped SnO NPs were then employed as photocatalyst for the photodegradation of MV dye in aqueous medium under UV irradiation. Further, the impact of different parameter like irradiation time, pH, recovered and recovered NPs, dye concentration and amount of photo catalyst were also studied. Density functional theory (DFT) calculations were also performed to explore the role of Mg atom doped into the crystal lattice of SnO on the optoelectronic properties.

2 Experimental

2.1 Materials

Analytical grade stannous chloride dehydrate **(**$SnCl_2 \cdot 2H_2O$), Nitric acid (HNO_3), Methyl violet dye (MV), Sodium hydroxide (NaOH) and Magnesium chloride hexahydrate ($MgCl_2.6H_2O$) were provided by Sigma Aldrich, German.

2.2 Preparation of Mg doped SnO NPs

Co-precipitation approach was adopted for the preparation of Mg doped SnO NPs.100 mL of each $MgCl_2.6H_2O$ (0.1 M) and $SnCl_2 \cdot 2H_2O$ **(**0.2 M) solutions were taken in reactor, then added NaOH solution (1 M) drop wise until the solution pH became basic and then heated at 80 °C for 3 h with continuous stirring. The mixture was then cooled and the obtained precipitates were separated via filtration. The obtained precipitates were washed several times with distilled water in order to remove any associated impurities. The prepared Mg doped SnO NPs were oven dried at 100 °C and stored for further use.

2.3 Photodegradation of Methyl violet dye

The synthesized doped NPs were employed as an effective photocatalyst for the degradation of MV dye under UV light irradiation in aqueous media, as a function of various operating parameters like irradiation time, photocatalyst dosage and dye initial concentration, and pH of the media. To achieve adsorption-desorption equilibrium, 10 mL (15 ppm) of MV dye and 0.02 g Mg doped SnO NPs were taken in 25 mL beaker and then placed it in the dark for 30 min. After the establishing of equilibrium, the dye solution was kept under UV light for designated period of time (5, 10, 15, 20 and 25 min keeping other parameters constant (10 mL MV solution and 0.02 g photocatalyst amount). After completion of the reaction time, the NPs were separated from the degraded solution through centrifugation. MV dye photodegradation studied was performed using UV-Vis spectrophotometer (Japan, UV-1800, Shimadzu). The following equation was used to determine % degradation of MV dye.

$$Degradation\ Rate\ (\%) = \frac{A_o - A}{A_o} \times 100$$

Where A_o and A denote the MV dye initial and final concentrations following photoreaction through UV light.

2.4 Theoretical study

We performed the entire calculations using the linearized augmented plane wave (FP-LAPW) method, which incorporates the Perdew-Burke-Ernzerhof (PBE) (Perdew et al. 1996) into the Density Functional Theory (DFT) employed in the WIEN2k package (Balaha et al. 2001).

The valence electronic configurations for Sn, Mg, and O atoms are $5s^25p^2$, $3s^2$, and $2s^22p^4$, respectively. Geometric/internal optimizations were performed using PBE, and the accuracy for

the self-consistent convergence was set to (1 mRy/au). The energy cut-off was considered up to 7.0. The electronic structure calculations were performed using the Trans-Blaha modified Becke Johnson approximation (TB-mBJ) (Koskelo et al. 2016), which mixes with the exchange of PBE functional. TB-mBJ is widely applied in calculating optoelectronic properties of oxides, which results in a suitable value of the band gap of these systems aligned with the experimental data. The Monkhorst-Pack k-sampling (Xinguo et al. 2013) of $6 \times 6 \times 4$ is used for pure/doped SnO to examine the effect of the k-grid on the density of states and valence/conduction band. Random phase approximation (RPA) (Tran and P Blaha] 2009) was used to calculate the optical spectra, utilizing the bands from the TB-mBJ approximation

2.5 Instrumentations

The morphology and FT-IR study of Mg doped SnO NPs was performed by SEM, JEOL, JSM-5910, SEM and Perkin Elmer, S.NO-95120, FT-IR, respectively. The purity and elemental composition of the prepared NPs was confirmed using EDX (Oxford instrument/EDX-INCA 200, UK, Oxford Company). Photodegradation study of MV dye was conducted through UV/Vis spectrophotometer (1800-UV, Shimadzu, Japan). The prepared NPs were also characterized by XRD (300/Model JEOL).

3 Result and discussion

3.1 Morphological and elemental composition study of Mg doped SnO NPs

Figure 1 illustrates the SEM micrograph of Mg doped SnO NPs, which present that the majority of NPs are cubic while shape of some particle are rounded. The NPs were also present in agglomerated form or aggregated. The SEM image also presented that NPs size are less than 100 nm while the average particle size of aggregates is around 440 nm. Figure 2 shows the elementals

and chemical composition of Mg doped SnO NPs. The spectrum shows Sn, Mg and O, which verified the synthesis of photocatalyst. The weight% of Sn, Mg and O are 76.85. 8.23 and 14.94% while the atomic% is 33.73, 17.64 and 48.64%, respectively. Further, the atomic and element weight% is also presented in the tubular form inside the figure 2.

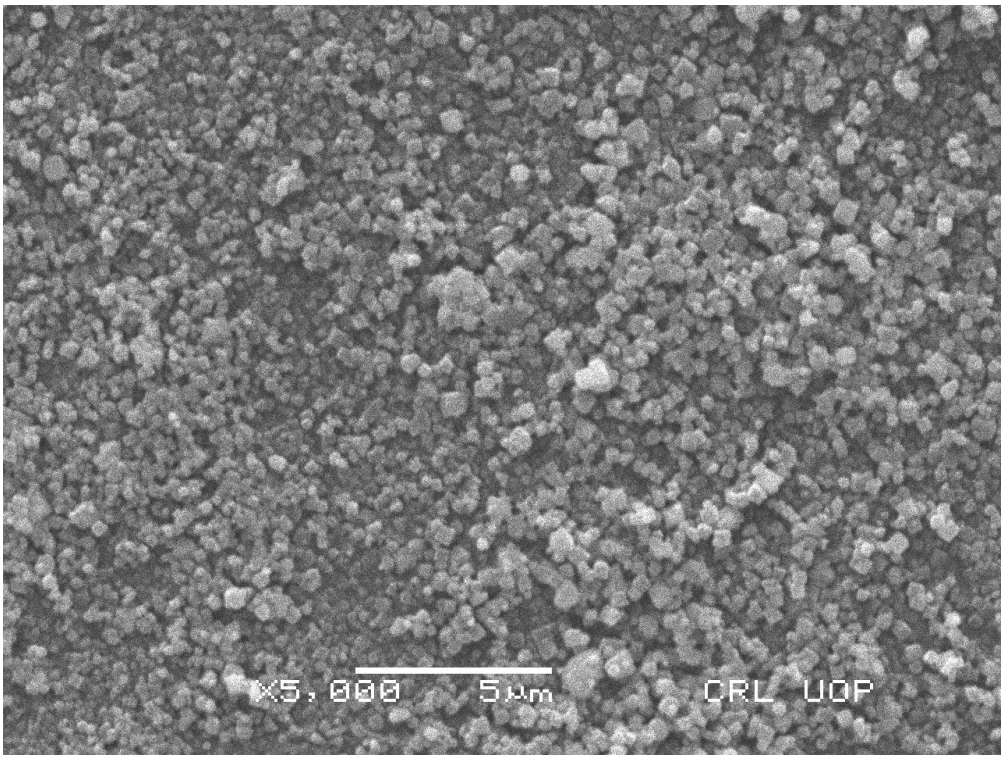


Figure 1: SEM analysis of Mg doped SnO NPs.

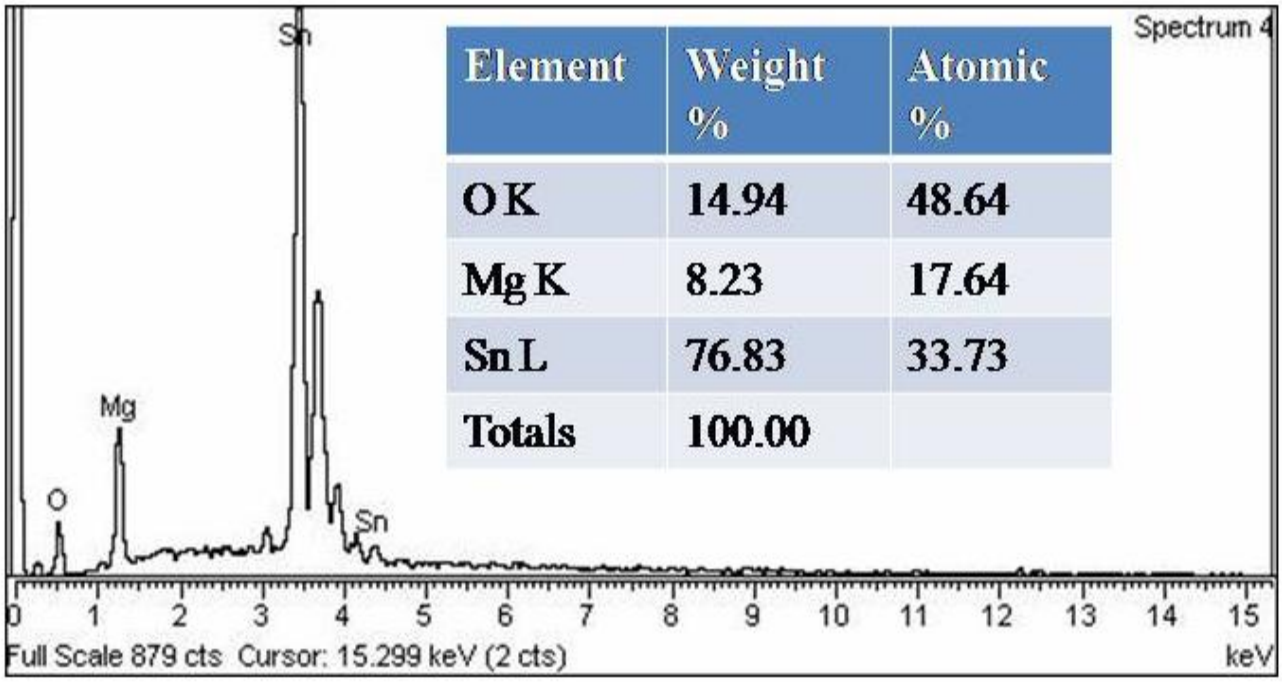


Figure 2: EDX spectrum of Mg doped SnO NPs.

3.2 FT-IR analysis of Mg doped SnO NPs

Figure 3 shows the FT-IR spectrum of Mg doped SnO NPs. The FT-IR spectrum presented peaks at 3173, 1167 and 1632 cm^{-1}, which might be due to the stretching and bending vibration of O-H bond derived from H_2O molecule that were absorbed on SnO surface (Asaithambi et al. 2020). The spectrum also gives peak at 530 cm^{-1}, which might be attributed to the stretching vibration of SnO. However, peaks were shifted to 753 and 833 cm^{-1} due to the successful doping of Mg in SnO NPs (Haspulat et al. 2020; v Farooq et al. 2013).

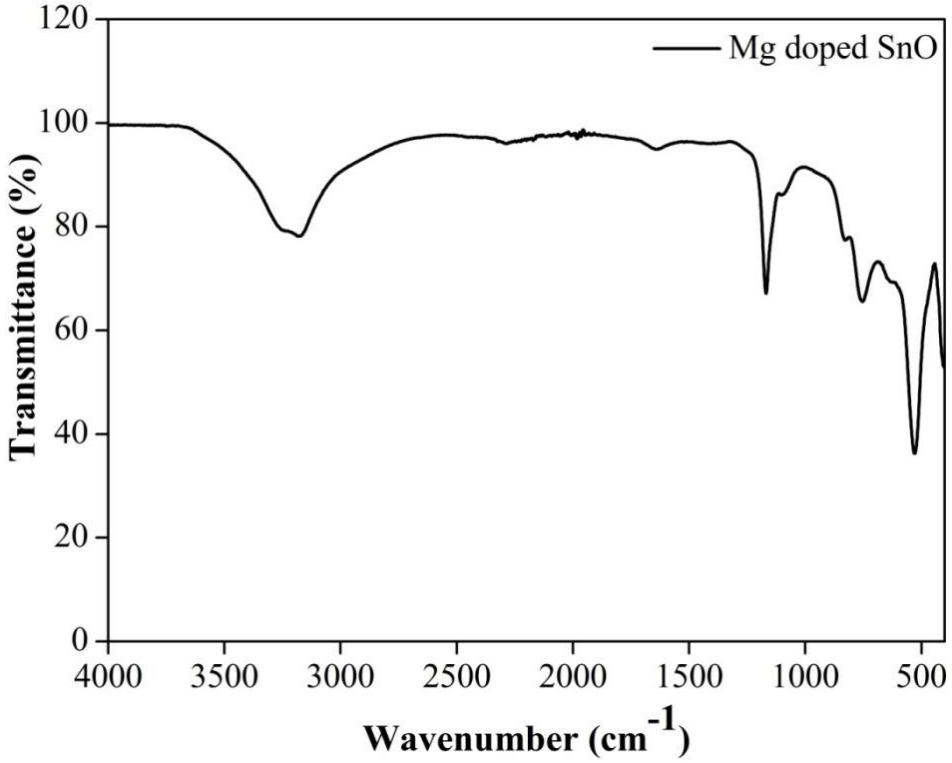


Figure 3: FT-IR spectra of Mg doped SnO NPs.

3.3 Band gap of Mg doped SnO NPs

Figure 4 demonstrate the band energy gap of the prepared NPs. Band gap energy of synthesized Mg doped SnO NPs was identified by employing Tauc plots mentioned in equation (1).

$$(\alpha hv)^2 = A\,(hv\text{-}Eg)^{m} \quad (1)$$

Where "α" is the absorbance, "h" stand for plank constant, "A" is energy independent constant, "v" is light incoming frequency, "Eg" is the value of optical band gap energy of NPs, and "hv" is the photon energy (Vignesh et al. 2019)]. By vertically extending "$(\alpha hv)^2$" curve to the horizontal X-axis, the direct "Eg" was estimated as 3 eV for Mg doped SnO, which is lower than from the reported value i.e., 3.1 and 3.4 eV of pure SnO (Liang et al. 2010: Hsu et al. 2014). However,

electron can be stimulated more readily from VB to CD band due to the smaller band gap, which result the decolonization/degradation of dye faster (Naz et al. 2023).

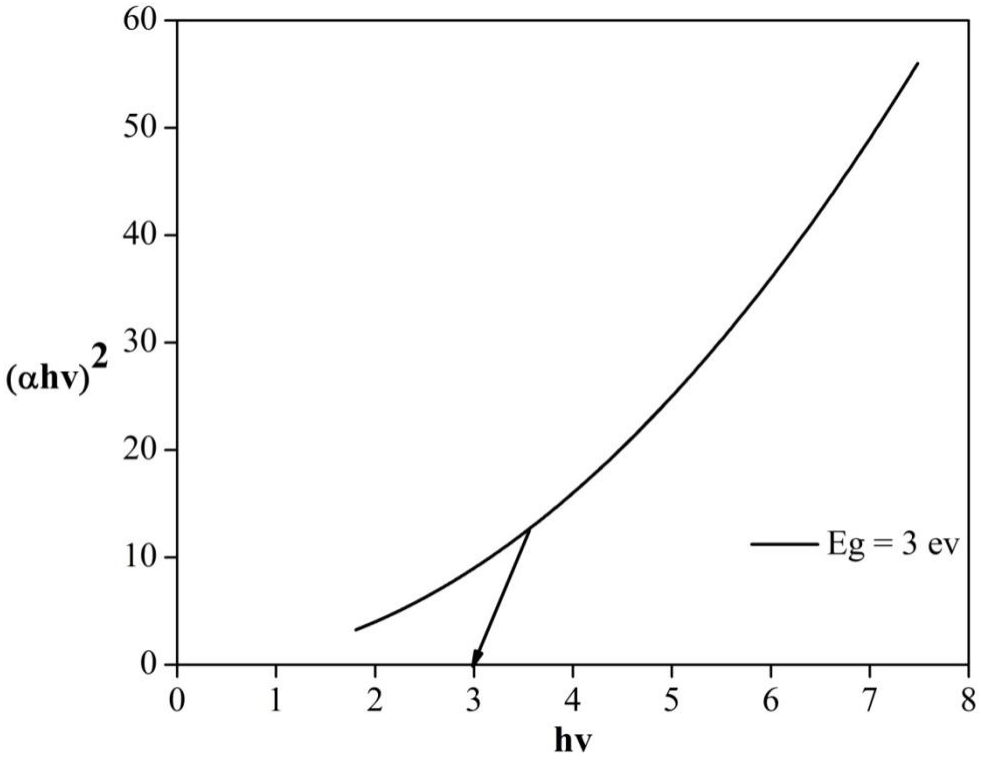


Figure 4: Band gap energy of Mg doped SnO.

3.4 XRD study

XRD analysis are mostly used to determine phase, crystal structure and orientation of NPs. Figure 5 depicts XRD spectrum of Mg doped SnO NPs. At angle (2 theta) value various bands or peaks can be observed at 19.8º, 22.9º, 32.6 º, 38.44, 40.2º, 46.7º, 52.7º and 58º, which were correspond to (111), (002), (022), (113), (222), (004), (024) and (224) planes. Crystallite size of the prepared Mg doped SnO NPs was found to be 0.10 nm, which was determined with the help of Scherer Debye equation from the intense peak in the XRD analysis. These various peaks match with COD (Reference-code No.96-901-1042) and also investigated that NPs are tetragonal in nature.

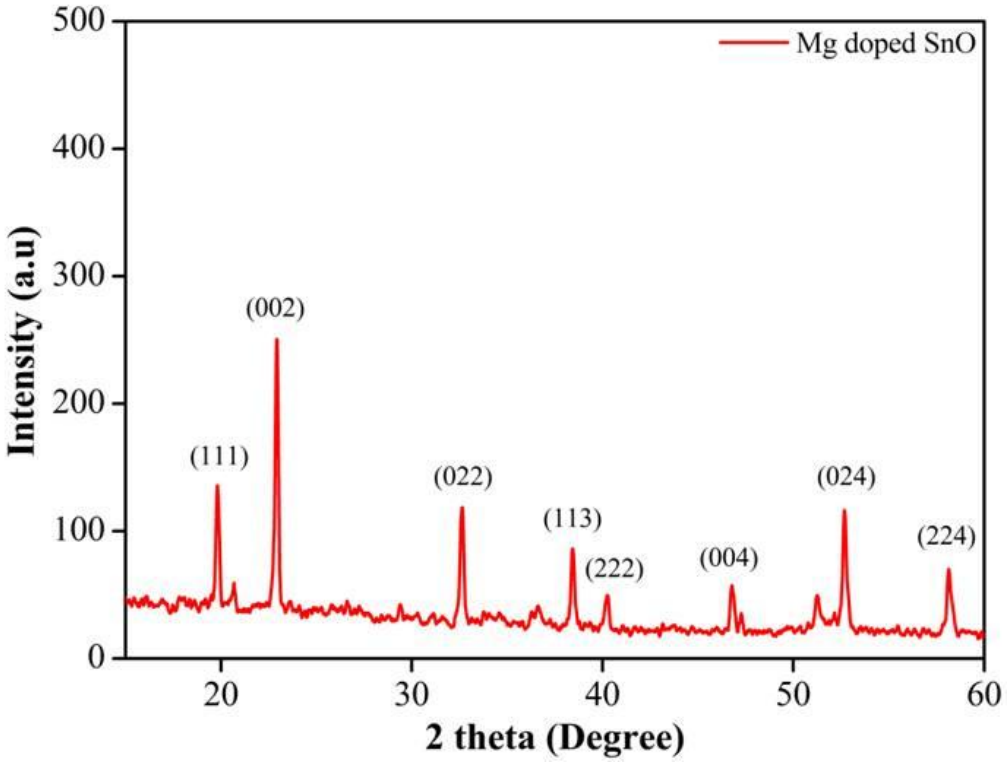


Figure 5: XRD analysis of Mg doped SnO NPs.

3.5 Photodegradation study of Methyl violet dye

3.6 Effect of Irradiation time on photodegradation of MV

The synthesized Mg doped SnO NPs were employed as photocatalyst in aqueous medium for the efficient removal of MV dye at different irradiation time (5, 10, 15, 20 and 25 min) while the catalyst amount (0.02 g) and dye concentration (15 ppm) were kept constant. The UV-Vis spectra and % degradation of MV in the presence of Mg doped SnO NPs are depicted in figure 6(a-b). The results show that the photodegradation of MV dye enhanced with enhancing irradiation time. Figure 6b presented that about 78 and 99.3% of dye degradation was achieved with irradiation time of 5 and 25 min, respectively. The rapid increase occurred in the photodegradation of MV

dye is due the rapid movement of electron from valence band to conduction band, which also results the formation of more electron hole pair (Barakat et al. 2011).

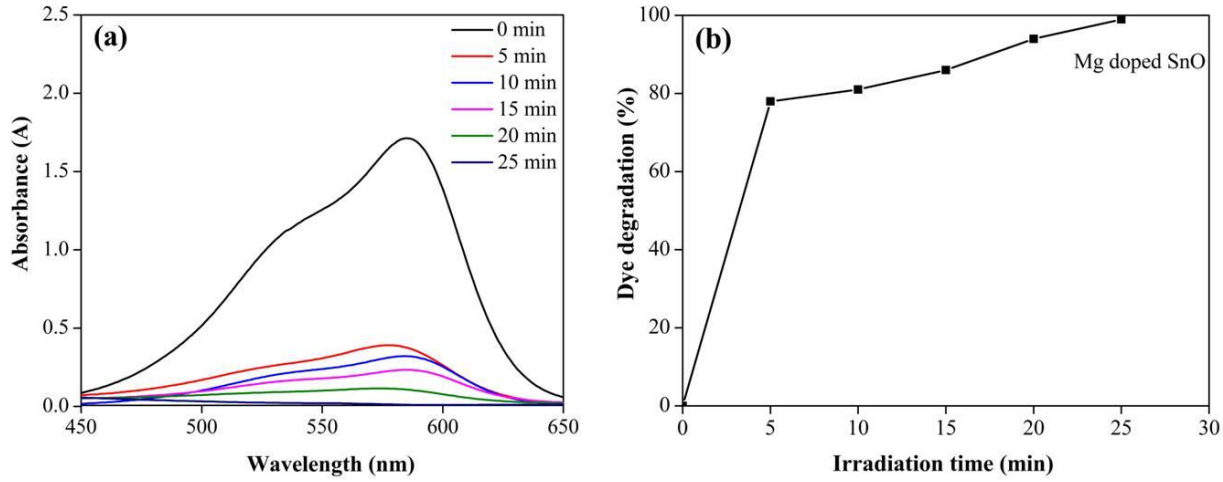


Figure 6:(a) UV/Vis spectra of MV dye degraded by Mg doped SnO (b) % degradation of MV

3.7 Kinetic study

The following mathematical equations were used to calculate pseudo first order and pseudo second order reaction of MV dye, which were photodegraded by Mg doped SnO NPs.

$$\ln(Co/C) = kKt = kt \qquad (2)$$

$$1/C - 1/Co = kt \qquad (3)$$

Where Co is initial and C is final concentration of dye, K is the coefficient of adsorption of the reactants and k is the reaction rate constantan. The data gives straight line by plotting ln(Co/C) and 1/C-1/Co against time, which demonstrate that slope is equal to k (apparent first order rate constant). Photodegradation kinetics of MV dye through Mg doped SnO NPs and the outcomes are illustrated in figure 7 a-b. The R^2 value of pseudo first order and pseudo second order kinetic

were 0.72017 and 0.41292 (Punithavathy et al. 2017), which indicated that the results were best fitted with pseudo first order kinetic.

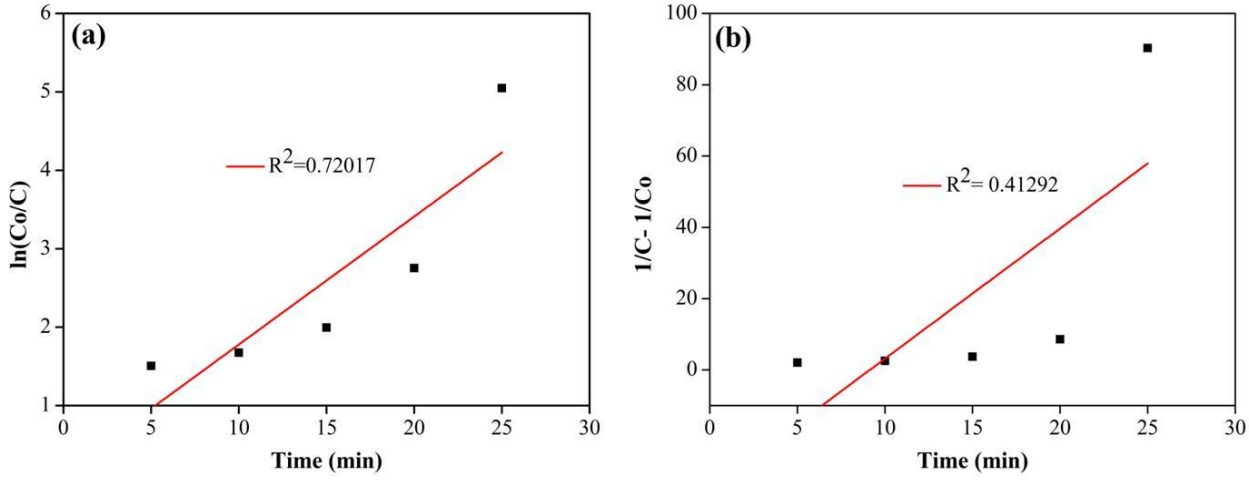


Figure 7: (a) First and (b) second order reaction of Mg doped SnO NPs.

3.9 Effect of catalyst amounts on degradation of MV dye

The impact of varying loading quantities of Mg doped SnO NPs i.e., 0.01, 0.15, 0.02, 0.025 and 0.03 g on the photodegradation of MV was also examined under fixed irradiation time 15 min and dye concentration 15 ppm. UV –Vis spectra and % degradation of MV dye are displayed in figure 8 (a-b). The findings demonstrated that the MV dye photodegradation improved with increasing Mg doped SnO NPs dosage from 0.01 to 0.03 g. According to the %degradation data, 0.01 g of Mg doped SnO degraded about 77% MV dye, which was enhanced up to 99% by loading to 0.03 g NPs. The enhancement of dye photodegradation can be explained by the fact that more photon adsorbed on the surface of NPs as the amount of photocatalyst increased and consequently large number of dye molecules adsorbed on the surface of NPs (Babel et al. 2016).

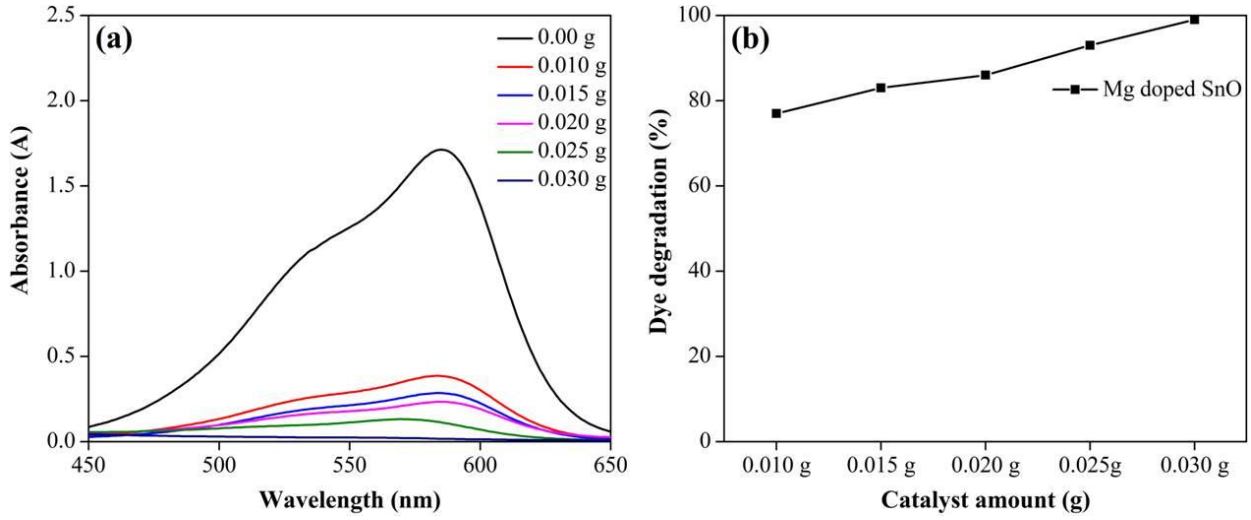


Figure 8: (a) UV-Vis spectra of MV dye (b) % degradation of MV dye degraded by Various amount of Mg doped SnO NPs.

3.10 Effect of initial concentration of dye

Initial contaminants concentration performs significant role in the photodegradation of organic dyes. The influence of starting concentration of MV dye on photodegradation rate was assessed by analyzing MV dye photocatalytic degradation using varying concentration (5, 10, 15, 20 and 25 ppm). This study is an important because the industries released organic dye at various concentrations while fixed the other parameters like catalyst dosage (0.02 g) and irradiation period (15 min). The percent degradation of MV dye in presence of Mg doped SnO NPs is shown in Figure 9. The results demonstrated at initial dye concentration of 5 ppm, 93% degradation of MV was attained in the presence of Mg doped SnO NPs, which was gradually decreased to 89, 86, 84 and 75% when the initial dye concentration was increased to 10, 15, 20 and 25 ppm, respectively. The decrease of dye degradation with the increase of initial dye concentration might be due to the large number of dye molecules adsorbed on surface of photocatalyst. The adsorbed dye molecules capture sufficient quantity of UV light instead of NPs surface and penetration of light to the

photocatalyst surface decrease, which result less production of •OH radical as dye occupy the available active site and thus the rate of photocatalytic degradation reduced (Reza et al. 2017).

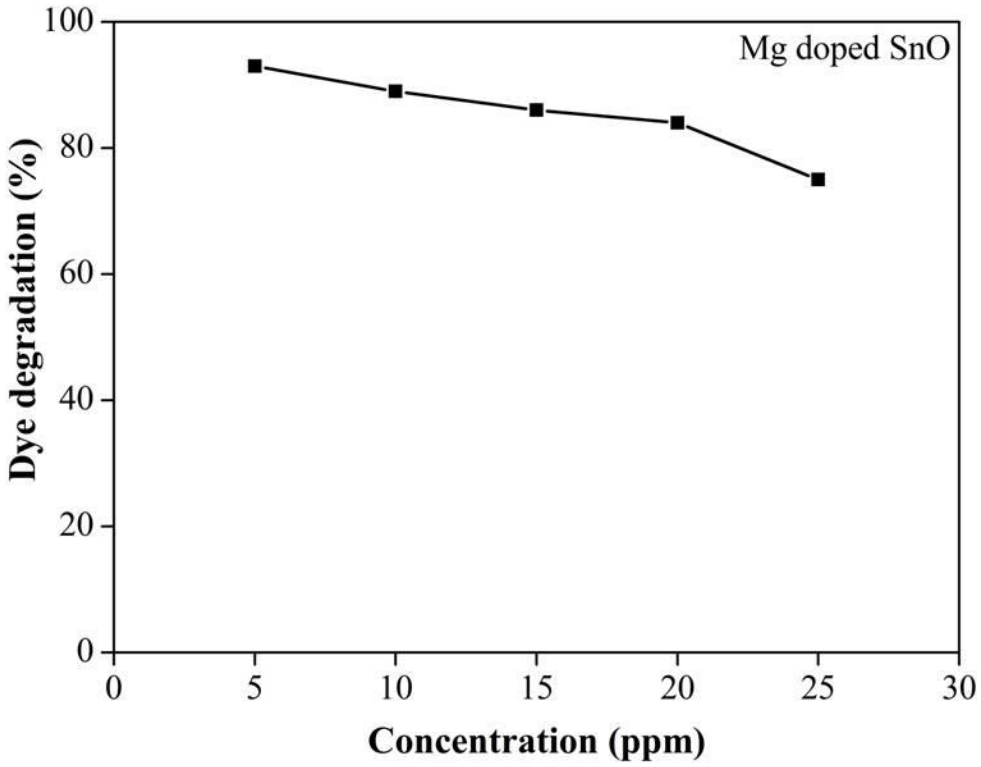


Figure 9: % degradation of MV dye using different initial dye concentration degraded by Mg doped SnO NPs

3.11 pH effect on the photodegradation of MV dye

The characteristics of chemical ions in the solution and surface feature of solid photocatalyst are significantly influenced the pH of the medium. As solution pH significantly affect photocatalytic degradation of organic dyes because different industries include textile leathers, papers and paints industries discharge their pollutants at different pH level. Thus at pH-3, pH-4 and pH- 5, the effect of pH on MV decomposition was investigated. The production of •OH radical and photochemical degradation of textile effluents are significantly influenced through pH level. Figure 10 illustrated the %degradation of MV dye and its relationship with pH of the medium. Percent degradation

study clearly display that as pH of the solution increase, the photodegradation of MV also increases. This can be explained by the fact that higher pH value causes more active •OH radicals, which speed up the decomposition rate of dye. The results presented that the photodegradation of MV was 74, 63 and 55% at pH -5, pH-4 and pH-3, respectively. While in the basic medium, MV dye is unstable and it degraded spontaneously i.e without the addition of Mg doped SnO NPs and UV light (Fu et al. 2018).

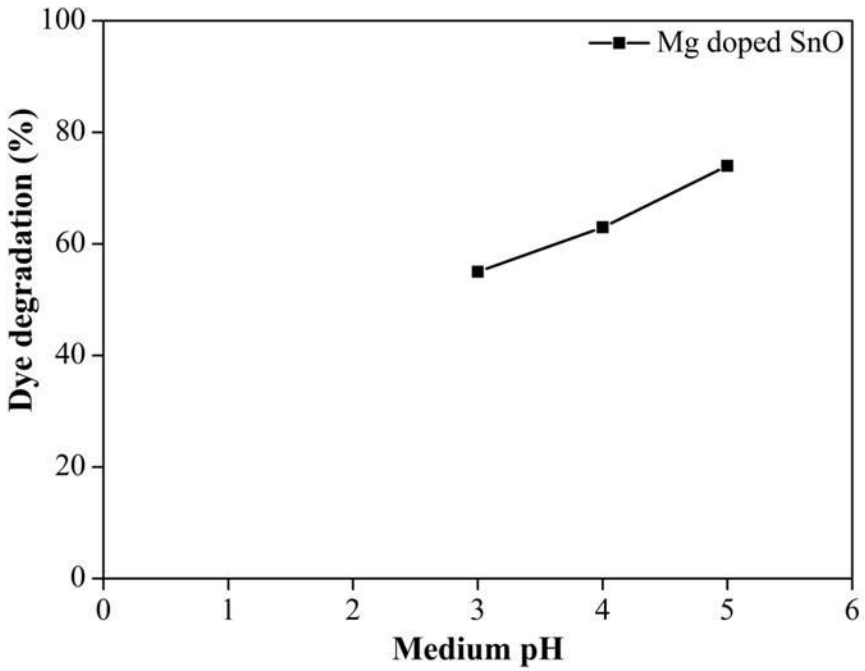


Figure 10: % degradation of MV dye via Mg doped SnO NPs at different pH value.

3.12 Effect of recovered and re-recovered NPs on photodegradation of MV dye

Utilizing recovered and re-recovered Mg doped SnO NPs and same experimental set up, the sustainability of NPs was also examined. Mg doped SnO NPs was isolated from MV solution via centrifugation and washed many time with double-distilled H_2O and dried at 100°C in oven. Figure 11 shows the UV-Vis spectra and %degradation of MV dye by recovered and re-recovered NPs,

which also significantly degraded the dye. The recovered NPs degraded 52 and 73% dye within 5 and 25 min while re-recovered NPs degraded 29 and 48% MV dye in 5 and 25 min under UV irradiation time, respectively.

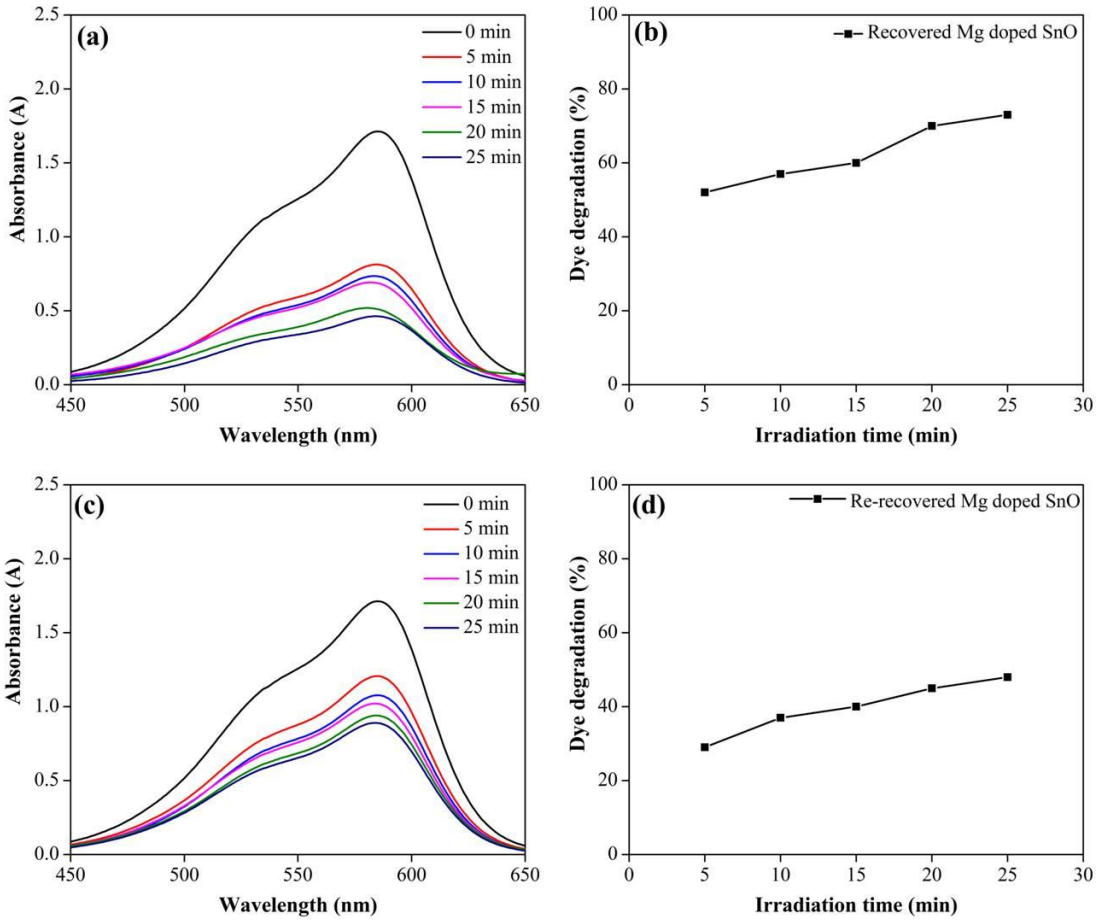
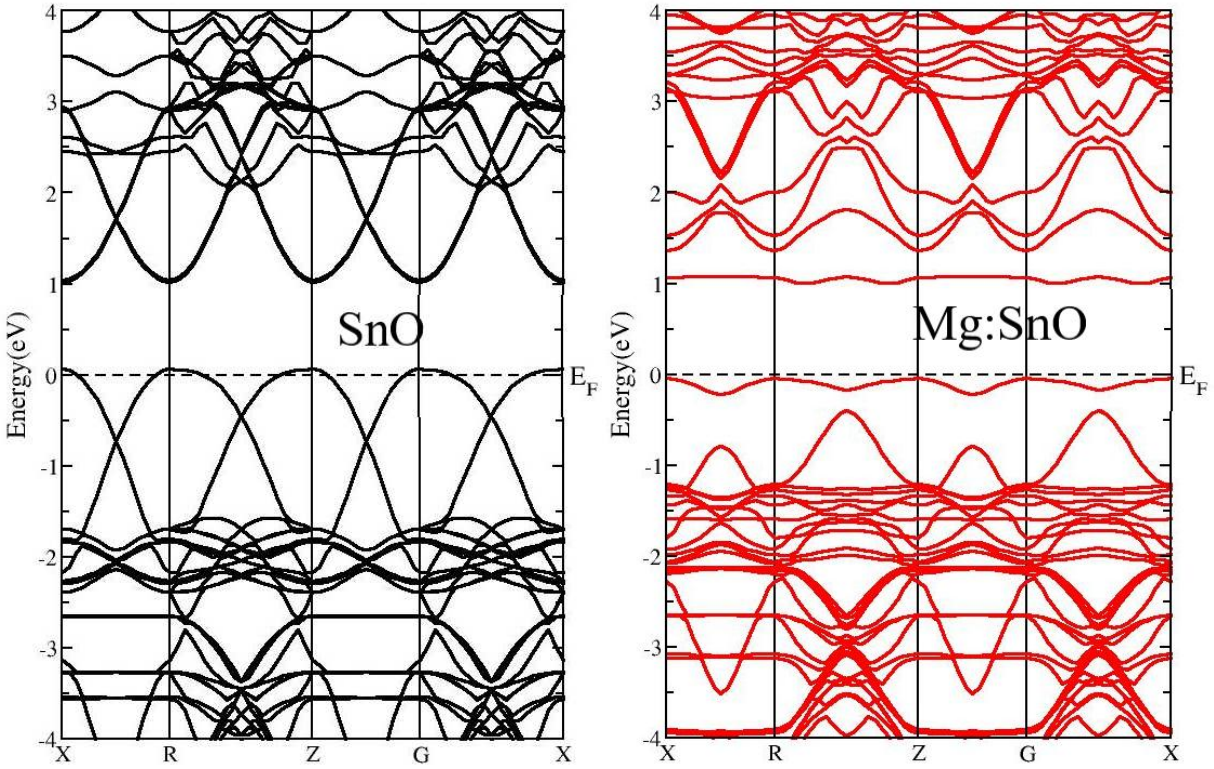


Figure 11:(a, c) UV-Vis spectra of recovered and recovered Mg doped SnO (b, d) % degradation of recovered and re-recovered NPs.

3.13 Electronic Structure

We calculated the band structures of pure and Mg-doped SnO using the TB-mBJ approximation, and the results are displayed in Fig. 12(a & b). For comparison with the Mg-doped system, the band structure calculation of the pure system was also performed for the same supercell ($2 \times 2 \times 1$

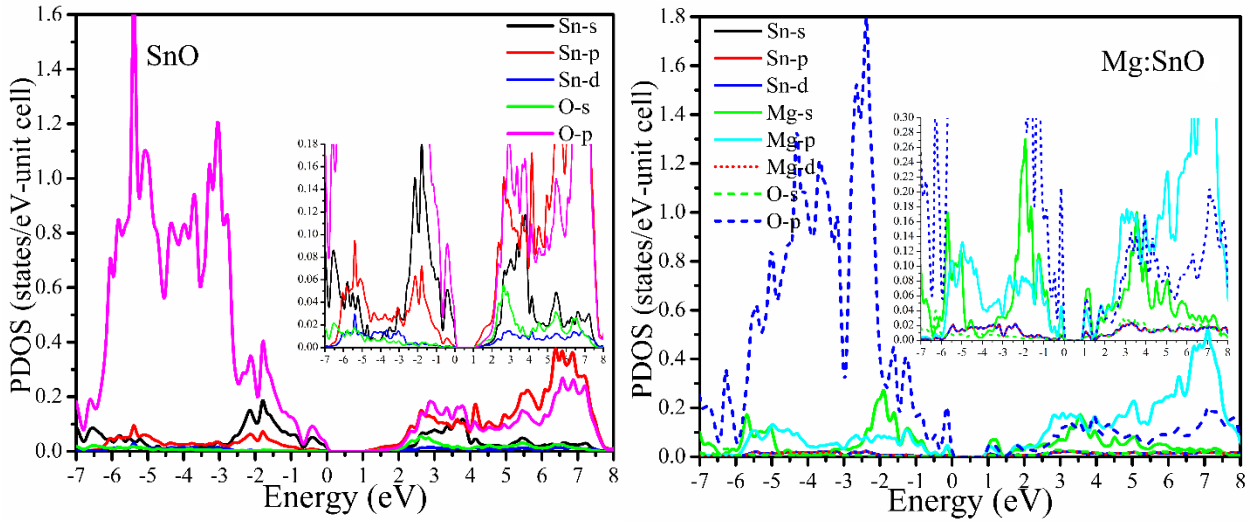
). The results reveal that the pure system is a direct band gap semiconductor, with a computed band gap of 1.129 eV. Fig. 12b depicts the calculated findings of the band structure of Mg-doped SnO, which reflects the indirect band gap behavior of the doped system. The red shift in the photovoltaic properties in the Mg-doped SnO is due to the creation of the localized mid-bands above the valence band and below the conduction band by the dopant Mg atom. The dopant also caused significant changes in the formation of valence/conduction bands of the doped system. Incorporating the non-metal (Mg) dopant could improve the photovoltaic properties of pure SnO by increasing light absorption in the infrared region.



(a) (b)

Figure. 12. Band structures of (a) SnO and (b) Mg-doped SnO using the Trans Blaha modified Becke Johnson approximation.

To better understand the passivation effect of Mg dopant in SnO, the partial density of states (PDOS) of pure/doped SnO, as displayed in Fig. The Fermi level is set to zero and is the highest occupied state/valence band. Compare the contributions of the relevant orbital to PDOS, and their corresponding overlapping are presented in Figs. 13 (a & b). Fig. 13a shows that the valence band edge of pure SnO is composed of the O p state and Sn s state, whereas the conduction band edge is predominantly composed of the Sn p state. In the VB, the region around -0.7 eV, and the region from -3.0 to -6.0, the O p state shows interplay with Sn s state, and the interplay has been observed between Sn s and O s states, respectively. The second Fig. 13b shows the PDOS of Mg-doped SnO. It is found that the introduction of Mg on the Sn lattice sites induces an intermediate state, contributed by the Mg s/p state, above the valence band maximum and below the conduction band minimum of the SnO. Interestingly, the dopant states are below the Fermi level, enhancing photovoltaic efficiency.



(a) (b)

Figure. 13 Partial density of states (PDOS) of (a) SnO and (b) Mg-doped SnO using the Trans Blaha modified Becke Johnson approximation

3.14 Absorption spectra

The calculated absorption ($\alpha(\omega)$) spectra of SnO/Mg-doped SnO are shown in Fig. 14. The calculated spectra depict the transparency region below the band gap when the radiation passes through that region of the studied systems. The findings of $\alpha(\omega)$ of pristine SnO/Mg-doped SnO reflect optical band gap values of 2.94 eV/0.94 eV. The optical absorption thresholds are positioned at 2.96 eV (SnO), and 0.96 eV (Mg:SnO). For the Mg-doped SnO, introducing the Mg atom into the lattice site of the pure crystal shifted the optical absorption to the infrared region. Calculated spectral peaks in Mg-doped SnO reveal a small peak in addition to the main peaks, attributed to impurity bands, while the remaining spectral behavior is similar.

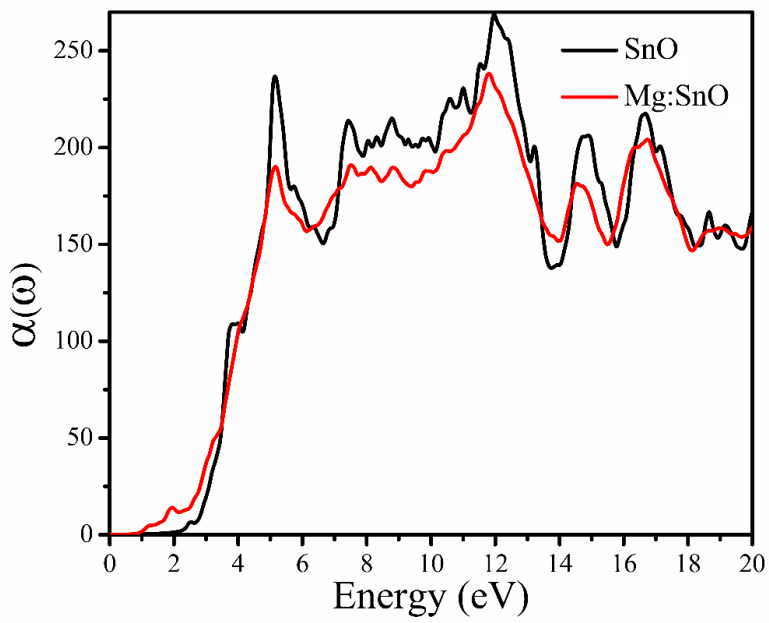


Figure. 14 Absorption spectra of SnO (black line) and Mg-doped SnO (red line) using the Trans Blaha modified Becke Johnson approximation

Conclusion

It was concluded that Mg-doped SnO exhibits incredible photocatalytic activity improvement in combination with ab-initio based calculations. The dopant shifted the optical absorption to the infrared region and the calculated optical band gap (3.0 eV) is aligned to the experimental one (3.0). It indicates the key role of Mg metal in facilitating the optoelectronic properties of pristine SnO. FT-IR analysis investigates whether the prepared NPs exist in their oxide form.SEM analysis shows that the average particle size is about 440 nm. The EDX spectrum suggests that no impurities can be found in the synthesized NPs. The theoretical study shows that the calculated band structure of Md-doped SnO revealed an intermediate band (sub-band) between the valence band and conduction band, which is assigned to the Mg atom in the crystal lattice of SnO. It was also found that the doped NPs were efficient photocatalysts for the photodegradation of MV dye. When irradiation time and photocatalyst amount increased, the MV dye photodegradation was also increased due to the formation of Hydroxyl radicals and the longer time availability of dye adsorption. At higher initial dye concentration, lower MV dye was degraded due to the accumulation of a large number of dye molecules adsorbed on the NPs surface and less penetration of light, and hence its photocatalytic activity of NPs is decreased.

References

Abdallah MAM, Alprol AE (2024) Utilization of aquatic bio mass as biosorbent for sustainable production of high surface area, nano-microporous, for removing two dyes from waste water. Sci Rep 14:447. DOI:10.1038/s41598-024-54539-2

Afzal MA, Javed M, Aroob S, Javed T, Alnoman MM, Alelwani W, Bibi I, Sharif M, Saleem M, Rizwan M, Raheel A, Maseeh I, Carabineiro SAC, Taj MB (2023) The Biogenic Synthesis of Bimetallic Ag/ZnO Nanoparticles: A Multifunctional Approach for Methyl Violet Photocatalytic Degradation and the Assessment of Antibacterial, Antioxidant, and Cytotoxicity Properties. Nanomater 13: 2079. DOI:10.3390/nano13142079

Aljuaid A, Almehmadi M, Alsaiari AA, Allahyani M, Abdulaziz O, Alsharif A, Alsaiari JA, Saih M, Alotaibi RT, Khan I (2023) g-C_3N_4 Based Photocatalyst for the Efficient Photodegradation of Toxic Methyl Orange Dye: Recent Modifications and Future Perspectives. Molecules 28: 3199. DOI:10.3390/molecules28073199

Al-Tohamy R, Ali SS, Li F, Okasha KM, Mahmoud YAG, Elsamahy T, Jiao H, Fu Y, Sun J (2022) A critical review on the treatment of dye-containing wastewater: ecotoxicological and health concerns of textile dyes and possible remediation approaches for environmental safety. Ecotoxicol Environ Saf 231:113160. https://doi.org/10.1016/j.ecoenv.2021.113160

Asaithambi S, Sakthivel P, Karuppaiah M, Hayakawa Y, Loganathan A, Ravi G (2020) Improved photocatalytic performance of nanostructured SnO via addition of alkaline earth metals (Ba^{2+}, Ca^{2+} and Mg^{2+}) under visible light irradiation. Appl Phys A Mater Sci process 126: 265. https://doi.org/10.1007/s00339-020-3441-8

Babel S, Sudrajat H, Abraham AA (2016) Manganese- and Iron-Doped Zinc Oxide for Photocatalytic Degradation of Recalcitrant Dyes. Thammasat Int J Sci Technol 21: 33-43. DOI 10.14456/tijsat.2016.28

Bagtache R, Djaballah AM, Tartaya S, Trari M (2022) Synthesis of $KCoPO_4$, physical and photoelectrochemical characterizations: application to the photodegradation of methyl violet. J Mater Sci Mater Electron 33:23682–23692. DOI:10.1007/s10854-022-09127-3

Bai MT, Anudeep YV, Raju CAI, Rao PV, Chittibabu N (2021) Decolourization of Eosin yellow (EY) dye using a variety of brown algae. Mater Today Proc 42:1130-1137. https://doi.org/10.1016/j.matpr.2020.12.495

Balaha P, Shewartz K, Madsen GKH, D. Kvsnicka, Luitz J (2001) WIEN2K, an Augmented Plane Wave +local Orbitals Program for Calculating Crystals Properties, ISBN 3-9501031-1-2, Karlheinz Schewartz, Techn. Universitat, Wien Austria.

Benkhaya S, Mrabet S, Harfi AE (2020) A review on classifications, recent synthesis and applications of textile dyes. Inorg Chem Commun 115: 107891. https://doi.org/10.1016/j.inoche.2020.107891

Benomara A, Guenfoud F, Mokhtari M, Boudjema A (2021) Sonolytic, sonocatalytic and sonophotocatalytic degradation of a methyl violet 2B using iron-based catalyst. React Kinet Mech Catal 132: 513-528. DOI:10.1007/s11144-020-01902-9

Barakat MA (2011) Adsorption and photodegradation of procion yellow H-EXL dyes in textile wastewater over TiO_2 suspension. J Hydro Environ Res 5:137-142. https://doi.org/10.1016/j.jher.2010.03.002

Cheng T, Gao H, Liu G, Pu Z, Wang S, Yi Z, Wu X, Yang H (2022) Preparation of core-shell hetero junction photocatalysts by coating CdS nanoparticles onto $Bi_4Ti_3O_{12}$ hierarchical microspheres and their photocatalytic removal of organic pollutant and Cr VI ions. Colloids Surf A Physicochem Eng Asp 633: 127918. https://doi.org/10.1016/j.colsurfa.2021.127918

Du C, Zhang Y, Zhang Z, Zhou L, Yu G, Wen X, Chi T, Wang G, Su Y, Deng F, Lv Y, Zhu H (2022) Fe-based metal organic frameworks (Fe-MOFs) for organic pollutants removal via

photo-Fenton: A review. J Chem Eng 431: 133932. https://doi.org/10.1016/j.cej.2021.133932

Elfiky AAEA, Mubarak MF, Keshawy M, Sayed IETE, Moghny TA (2024) Novel nano filtration membrane modified by metal oxide nanocomposite for dyes removal from wastewater. Environ Dev Sustain 26: 19935–19957. https://doi.org/10.1007/s10668-023-03444-1

Farooq WA, Ali SM, Muhammad J, Ali SD, Aziz MH, Ur-Rehman N Hussain M (2013) Synthesis and characterization of $Sn_1Mg_{1-x}O_2$ thin films fabricated by aero-sole assisted chemical vapor deposition. J Mater Sci Mater Electron 24: 5140–5146. https://doi.org/10.1007/s10854-013-1536-0

Fu H, Yang Y, Zhu R, Liu J, Usman M, Chen Q, He H (2018) Superior adsorption of phosphate by ferrihydrite-coated and lanthanum-decorated magnetite. J Colloid Interface Sci 530: 704-713. https://doi.org/10.1016/j.jcis.2018.07.025

Gul T, Saeed K, Ahmad S, Almehmadi M, Alsaiari AA, Alsharif A, Khan I (2023) Investigation of the photocatalytic and biological applications of iron oxide–indium oxide nanocomposite. Chem Pap 77: 4547-4558. https://doi.org/10.1007/s11696-023-02805-4

Haleem A, Shafiq A, SQ Chen, Nazar M (2023) A Comprehensive Review on Adsorption, Photocatalytic and Chemical Degradation of Dyes and Nitro-Compounds over Different Kinds of Porous and Composite Materials. Molecules 28: 1081. DOI:10.3390/molecules28031081

Hsu PC, Hsu CJ, Chang CH, Tsai SP, Chen WC, Hsieh HH, Wu CC (2014) Sputtering Deposition of P-Type SnO Films with SnO Target in Hydrogen-Containing Atmosphere. ACS Appl Mater Interfaces 6: 13724-13729. DOI: 10.1021/am5031787

Hamza M, hedi RA, Brillas E, Sires I (2009) Comparative electrochemical degradation of the triphenylmethane dye Methyl Violet with boron-doped diamond and Pt anodes. J Electroanal Chem 627: 41–50. https://doi.org/10.1016/j.jelechem.2008.12.01

Haspulat B, Sarıbel M, Kams H (2020) Surfactant assisted hydrothermal synthesis of SnO nanoparticles with enhanced photocatalytic activity. Arab J Chem 13: 96-108. https://doi.org/10.1016/j.arabjc.2017.02.004

Kadhom M, Albayati N, Alalwan H, Al-Furaiji (2020) M Removal of dyes by agricultural waste. Sustain Chem Pharm 16: 100259. https://doi.org/10.1016/j.scp.2020.100259

Karthik KV, Raghu AV, Reddy KR, Ravishankar R, Sangeeta M, Shetti NP, Reddy NCV (2022) Green synthesis of Cu-doped ZnO nanoparticles and its application for the photocatalytic degradation of hazardous organic pollutants. Chemosphere 287: 132081. https://doi.org/10.1016/j.chemosphere.2021.132081

Kaur M, Pahwa C, Sharma R, Jindal S (2024) Natural sunlight assisted photocatalytic removal of methylene blue and crystal violet dyes using Ni doped tin oxide nanostructures synthesized via chemical and green route. Appl Phys 130: 333. https://doi.org/10.1007/s00339-024-07500-z

Khan N, Gul T, Khan I, Saeed K (2024) Improvement of the Photocatalytic and Biological Activities of Copper Oxide Nanoparticles by Coupling with Barium Oxide Nanoparticles. Bio Nano Science 14: 710–724. https://doi.org/10.1007/s12668-024-01449-2

Keyhanian F, Shariati S, Faraji M, Hesabi M (2016) Magnetite nanoparticles with surface modification for removal of methyl violet from aqueous solutions. Arab J Chem 9: S348–S354.

Khorasanizadeh MH, Oghaz MH, Khoobi A, Ganduh SH, Mahdi MA, Abdulsahib WK, Jasim LS, Niasari MS (2022) Synthesis and characterization of $HoVO_4$/CuO nanocomposites for

photodegradation of methyl violet. Int J Hydrogen Energy 47: 20112-20128. https://doi.org/10.1016/j.ijhydene.2022.04.136

Koskelo J, Hashemi J, Huotari S, Hakala M (2016) Koskelo J, Hashemi J, Huotari S, Hakala M (2016) First-principles analysis of the intermediate band in $CuGa_{1-x}Fe_xS_2$. Physical Review B 93: 165204. https://doi.org/10.1103/PhysRevB.93.165204

Kumari H, Sonia, Suman, Ranga R, Chahal S, Devi S, Sharma S, Kumar S, Kumar P, Kumar S, Kumar A, Parmar RA (2023) Review on photocatalysis used for wastewater treatment: dye degradation. Water Air Soil Pollut 234: 349. https://doi.org/10.1007/s11270-023-06359-9

Ledakowicz S, Pa´zdzi K (2021) Recent achievements in dyes removal focused on advanced oxidation processes integrated with biological methods. Molecules 26: 870. https://doi.org/10.3390/molecules26040870

Leilakouhi BA, Jangi SRH, Khorshidi A (2023) Introducing a novel photo-induced nanozymatic method for high through put reusable biodegradation of organic dyes. Chem Pap 77: 1033–1046. https://doi.org/10.1007/s11696-022-02542-0

Liang LY, Liu ZM, Cao HT, Pan XQ (2010) Microstructural, Optical, and Electrical Properties of SnO Thin Films Prepared on Quartz via a Two-Step Method. ACS Appl Mater Interfaces 2: 1060-1065. DOI:10.1021/am900838z

Mandal RK, Saha P, Majumder TP (2021) Structural, optical characterization of the synthesized Fe doped CdO Nano particles, its application as a promising photocatalyst for degradation of the hazardous Methyl violet dye. Optik 246: 167795. https://doi.org/10.1016/j.ijleo.2021.167795

Mecha AC, Chollom MN (2020) Photocatalytic ozonation of wastewater: a review. Environ Chem Lett 18: 1491-1507. https://doi.org/10.1007/s10311-020-01020-x

Moradkhanloo SK, Baghdadi M, Torabian A (2023) Enhanced photocatalytic NOM removal in photo-assisted coagulation-flocculation process using TiO_2 nano-catalyst coated on settling tank. Int J Environ Sci Technol 20: 3661–3672. https://doi.org/10.1007/s13762-023-04807-x

Naz F, Nabi GAK, Nawaz A, Ali S, Siddique M (2023) A Novel Approach for the Photocatalytic Degradation of Binary Dyes Mixture Using SnO Nanoparticles as a Catalyst. J Clust Sci 34: 2047-2066. DOI:10.1007/s10876-022-02367-7

Negash A, Tibebe D, Mulugeta M, Kassa Y (2023) A study of basic and reactive dyes removal from synthetic and industrial wastewater by electrocoagulation process. S Afr J Chem Eng 46: 122–131. https://doi.org/10.1016/j.sajce.2023.07.015

Oyarce E, Butter B, Santander P, Sánchez J (2021) Polyelectrolytes applied to remove methylene blue and methyl orange dyes from water via polymer-enhanced ultrafiltration. J Environ Chem Eng 9: 106297. https://doi.org/10.1016/j.jece.2021.106297

Perdew JP, Burke K, Ernzerhof M (1996) Generalized gradient approximate made simple. Phys Rev Lett 77, 3865. https://doi.org/10.1103/PhysRevLett.77.3865

Pirzada T, Kanhar FH, Talpur MMA, Chandio WA, umani Z, Chandio IA (2021) An Effective Photocatalytic degradation of Rose Bengal and Eosin Y by Using ZnO Nanoparticles as a Photocatalysts. Ann Rom Soc Cell Biol 25: 1473-1488.

Punithavathy K, Richard JP, Jeyakumar SJ, Jothibas M, Praveen P (2017) Photodegradation of methyl violet dye using ZnO nanorods. J Mater Sci Mater Electron 28: 2494–2501. DOI 10.1007/s10854-016-5823-4

Quintero JDA, García MAGO, G´omez ID (2024) The scope of alum coagulation-flocculation assisted by slaked lime for the treatment of industrial wastewater containing highly

concentrated Acid Black 194 dye. Optimization, molecular weight distribution and toxicity analysis. Results Eng 23: 102676. https://doi.org/10.1016/j.rineng.2024.102676

Reza KM, Kurny A, Gulshan F (2017) Parameters affecting the photocatalytic degradation of dyes using TiO_2: a review. Appl Water Sci 7: 1569–1578. DOI 10.1007/s13201-015-0367-y

Rezeki YT, Zainul R (2024) Harnessing Cu-Doped ZnO for the photo transformation of methyl violet: a comprehensive review on synthesis, mechanisms, and catalytic potency. Electrolyte 3: 2828-3147. https://doi.org/10.54482/electrolyte.v3i1.274

Sabouri Z, Sabouri M, Moghaddas SSTH, Mostafapour A, Samarghandian S, Darroudi M (2023) Plant-mediated synthesis of Ag and Se dual-doped ZnO-CaO-CuO nanocomposite using Nymphaea alba L. extract: Assessment of their photocatalytic and biological properties. Biomass Convers Biorefin. 13, 2190-6823. https://doi.org/10.1007/s13399-023-04984-2

Saeed M, Albalawi K, Khan I, Akram N, El-Rahim IHAA, Alhag SK, Ahmed AE, Faiza (2023) Synthesis of p-n NiO-ZnO heterojunction for photodegradation of crystal violet dye. Alex Eng J 65: 561–574. https://doi.org/10.1016/j.aej.2022.09.048

Saini K, Sahoo A, Kumar J, Kumari A, Pant KK, Bhatnagar A, Bhaskar T (2023) Effective utilization of discarded reverse osmosis post-carbon for adsorption of dyes from waste water. Environ Res 231: 116165. https://doi.org/10.1016/j.envres.2023.116165

Tran F, Blaha P (2009) Accurate band gaps of semiconductors and insulators with a semilocal exchange-correlation potential Phys Rev Lett 102: 226401. DIO:10.1103/Physrevlett.102.226401

Vignesh G, Rajesh G, Kumar MK (2021) Mn, Mg-doped ZrO_2 nanoparticles: a photo stable catalyst for enhanced mineralization and photocatalytic degradation of MV and MB dyes under sunlight irradiation. J Mater Sci Mater Electron 32: 27044–27059. https://doi.org/10.1007/s10854-021-07076-x

Vignesh S, Suganthi S, Sundar JK, Raj V, Devi PRI (2019) Highly efficient visible light photocatalytic and antibacterial performance of PVP capped Cd:Ag: ZnO photocatalyst nanocomposites. Appl Surf Sci 479: 914-929. https://doi.org/10.1016/j.apsusc.2019.02.064

Wang F, Xu J, Wang Z, Lou Y, Pan C, Zhu Y (2022) Unprecedentedly efficient mineralization performance of photocatalysis- self-Fenton system towards organic pollutants over oxygen-doped porous g-C_3N_4 nanosheets. Appl Catal B Environ 312: 121438. https://doi.org/10.1016/j.apcatb.2022.121438

Ma X, Wu Y, Lv Y, Zhu Y J (2013) Correlation Effects on Lattice Relaxation and Electronic Structure of ZnO within the GGA+*U* Formalism Phys Chem C 117: 26029−26039.

Yaseen DA, Scholz M (2019) Textile dye wastewater characteristics and constituents of synthetic effluents: a critical review. Int J Environ Sci Technol 16: 1193–1226. https://doi.org/10.1007/s13762-018-2130-z

Acknowledgements

This research was supported by the Bacha Khan University Charsadda

Author contribution

Nisar Khan: methodology, analysis and preparation of manuscript. Tamanna Gul: guidance, reviewing and editing the manuscript. Falak Naz: data curation and editing the manuscript. Wilayat Khan: Theoretical, assisted in the methodology, and editing the manuscript. Sikander Azam: Theoretical study and review the manuscript. Khalid Saeed: supervision, guidance, reviewing, editing, and endorsed the final manuscript.

Funding

This study received no funding

Data availability

The authors declare that the data supporting the findings of this study are available within the paper.

Declarations

Conflict of interest

The authors declare no conflict of interest.

Ethical approval

This is not applicable.

Consent for publication

This study does not include any individual person's data in any form, and therefore, consent to publish is not applicable